TUDelft

Delft University of Technology

Effect of Dispersing Solvents for an Ionomer on the Performance of Copper Catalyst Layers for CO$_2$ Electrolysis to Multicarbon Products

Idros, Mohamed Nazmi; Wu, Yuming; Duignan, Timothy; Li, Mengran; Cartmill, Hayden; Maglaya, Irving; Burdyny, Thomas; Wang, Geoff; Rufford, Thomas E.

Important note
To cite this publication, please use the final published version (if applicable).
Please check the document version above.

Effect of Dispersing Solvents for an Ionomer on the Performance of Copper Catalyst Layers for CO$_2$ Electrolysis to Multicarbon Products

Mohamed Nazmi Idros, Yuming Wu, Timothy Duignan, Mengran Li,* Hayden Cartmill, Irving Maglaya, Thomas Burdyny, Geoff Wang, and Thomas E. Rufford*

ACCESS | Metrics & More | Article Recommendations | SI Supporting Information

ABSTRACT: To explore the effects of solvent−ionomer interactions in catalyst inks on the structure and performance of Cu catalyst layers (CLs) for CO$_2$ electrolysis, we used a "like for like" rationale to select acetone and methanol as dispersion solvents with a distinct affinity for the ionomer backbone or sulfonated ionic heads, respectively, of the perfluorinated sulfonic acid (PFSA) ionomer Aquivion. First, we characterized the morphology and wettability of Aquivion films drop-cast from acetone- and methanol-based inks on flat Cu foils and glassy carbons. On a flat surface, the ionomer films cast from the Aquivion and acetone mixture were more continuous and hydrophobic than films cast from methanol-based inks. Our study's second stage compared the performance of Cu nanoparticle CLs prepared with acetone and methanol on gas diffusion electrodes (GDEs) in a flow cell electrolyzer. The effects of the ionomer−solvent interaction led to a more uniform and flooding-tolerant GDE when acetone was the dispersion solvent (acetone-CL) than when we used methanol (methanol-CL). As a result, acetone-CL yielded a higher selectivity for CO$_2$ electrolysis to C$_{2+}$ products at high current density, up to 25% greater than methanol-CL at 500 mA cm^{-2}. Ethylene was the primary product for both CLs, with a Faradaic efficiency for ethylene of 47.4 $\pm$ 4.0% on the acetone-CL and that of 37.6 $\pm$ 5.5% on the methanol-CL at a current density of 300 mA cm^{-2}. We attribute the enhanced C$_{2+}$ selectivity of the acetone-CL to this electrode's better resistance to electrolyte flooding, with zero seepage observed at tested current densities. Our findings reveal the critical role of solvent−ionomer interaction in determining the film structure and hydrophobicity, providing new insights into the CL design for enhanced multicarbon production in high current densities in CO$_2$ electrolysis processes.

KEYWORDS: electrochemical CO$_2$ reduction, perfluorinated sulfonic acid (PFSA) ionomer, catalyst ink formulation, solubility parameter, Aquivion conformation
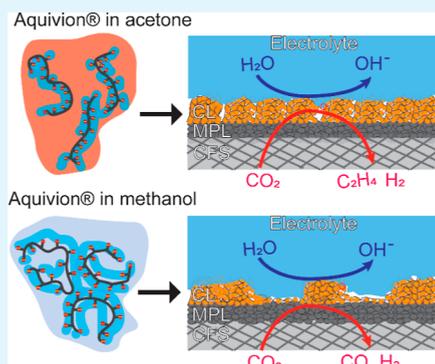
1. INTRODUCTION

Electrolysis powered by renewable electricity is a potential technology to convert industrial carbon dioxide (CO$_2$) emissions into chemicals and fuels.[1,2] Copper (Cu) is one of the most promising catalysts for CO$_2$ electrolysis to multicarbon products (C$_{2+}$ products), such as ethylene and ethanol,[3−5] at low temperatures and industrially relevant current densities.[6] For example, flow cell electrolyzers using Cu catalysts supported on a gas diffusion layer (GDL) have been reported to achieve selectivity (Faradaic efficiency) for CO$_2$ electrolysis to C$_{2+}$ products of more than 65% at current densities greater than 200 mA cm^{-2}.[7,8] The structure of the gas diffusion electrode (GDE) enables fast CO$_2$ mass transfer through a GDL and provides a high density of active sites in the catalyst layer (CL).[9−12] Further, the CL's morphology and composition impact the reaction conditions at the cathode, affecting CO$_2$ electrolysis selectivity toward desired products, suppressing or promoting the hydrogen evolution reaction (HER) and influencing the stability of the CO$_2$ electrolyzer.[11−13]

The prevailing method to fabricate a CL on the GDL in the CO$_2$ electrolysis literature is spray coating or blade coating[12] an ink containing a dispersion of catalyst particles, ionomer, and binders in a solvent such as isopropyl alcohol (IPA) or acetone.[7,8,14] Commonly, the ionomer is a perfluorinated sulfonic acid (PFSA) copolymer composed of a polytetrafluoroethylene (PTFE) backbone (e.g., $-[CF_2-CF_2]_x-$) tethered with perfluoropolyether pendant side chains that terminate with a sulfonic group (e.g., $-O-CF_2-CF_2-SO_3H$)[15,16] (Figure 1a). The ionomer's hydrophilic sulfonic acid side chains help bind the catalyst particles onto the GDL and promote ion transport across catalyst−electrolyte interfaces.[8] The PTFE backbones provide hydrophobic pathways
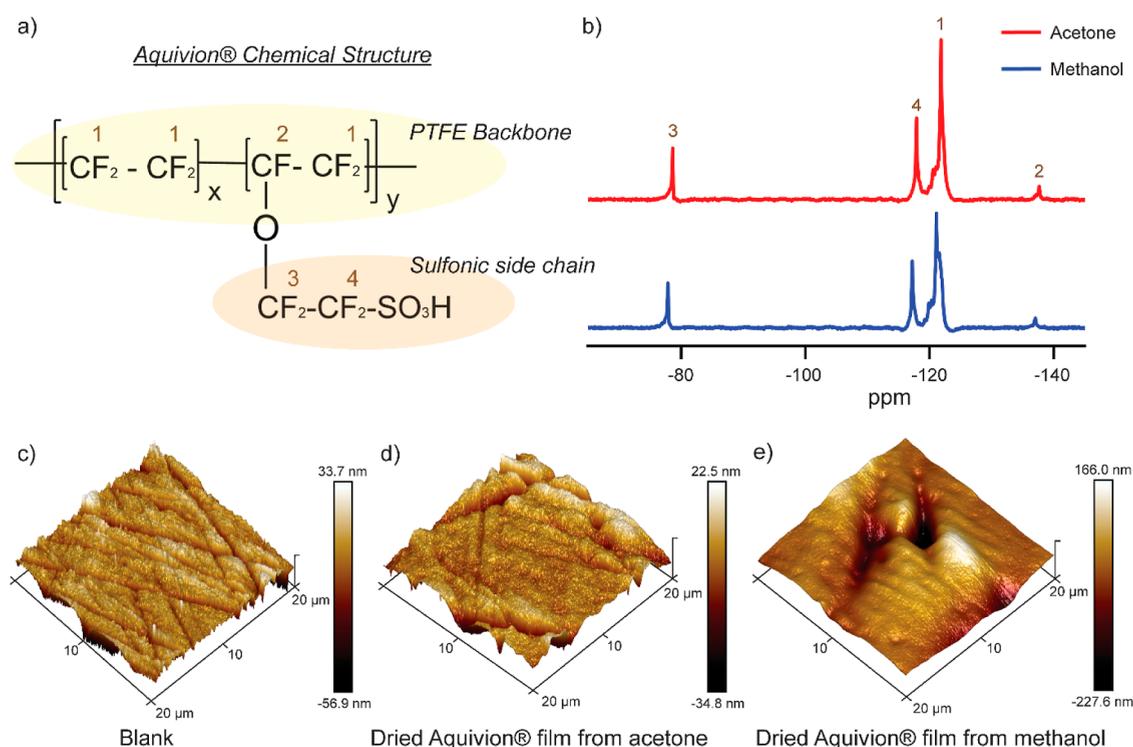
Figure 1. Comparison of PFSA biphasic interactions in solvents with distinct solubility parameters and its morphology on flat surfaces. (a) Aquivion chemical structure with the PTFE backbone and side chain labeled. (b) 19-Fluorine (^{19}F) NMR spectrum for 1 g L^{-1} Aquivion in acetone and methanol. The NMR spectra peaks in (a) are labeled based on Johnston et al.[34] To simplify, peak 1 represents the Aquivion backbone, while peaks 3, 4, and 2 represent the Aquivion side chains. AFM images of (c) a clean blank Cu foil and of Cu foils coated with the dried Aquivion film fabricated by casting Aquivion dispersed in (d) acetone and (e) methanol at Aquivion with a concentration of 20 g L^{-1}. The ionomer loading is 40 $\mu g\ cm^{-2}$.

for the percolation of gas reactants and products.[8,14,17−19] Given these properties, the conformation of ionomer molecules in the catalyst ink can impact the structure of the CL and, ultimately, affect the performance of the electrode for CO_2 electrolysis.[14,20,21]

Although there are few studies on ionomer−solvent interactions for CO_2 electrolysis,[21] we can learn from prior studies of solvent selection in fabricating CLs for proton exchange membrane (PEM) fuel cells.[22−29] For example, Hoffman et al. concluded in a study with the short side chain PFSA Aquivion and binary solvent mixtures of water and diacetone alcohol that solvent properties govern ionomer conformation in the catalyst ink, and consequently, the solvent choice can influence the final properties and performance of the CL.[30] A critical factor affecting the conformation of ionomers in catalyst ink is the relative solubility difference between the ionomer's PTFE backbone, sulfonated ionic heads, and solvent. As summarized in Table 1, ionomer PTFE backbones have a lower solubility parameter than the sulfonated ionic head groups.[15,26] Thus, the PTFE backbone synergically swelled in solvents with a low solubility parameter (e.g., acetone, 9.9 cal$^{0.5}$ cm$^{1.5}$) than in a solvent with a higher solubility parameter (e.g., methanol, 14.5 cal$^{0.5}$ cm$^{1.5}$),[31] which leads to the unfolding of the ionomer backbone into the solvent when a low solubility parameter solvent is used in the catalyst ink. Conversely, dispersion of the ionomer in a solvent with high solubility parameters such as methanol leads to densely packed ionomer structures with greater ionic clusters.

To explore the effects of solvent−ionomer interactions in catalyst ink on the structure and performance of Cu CLs for

Table 1. Summary of Solubility Parameters for Solvents and Ionomer Use in the Catalyst Ink Formulation[a]

solvent	Hildebrand solubility (cal$^{0.5}$ cm$^{1.5}$)	boiling point (°C)
acetone	9.9	56.1
N-methylformamide	16.1	93.0
methanol	14.5	64.5
isopropanol	11.5	82.2
ethanol	12.7	78.24
water	23.4	100.0
Nafion[b] (EW: 1100 g mol^{-1})	10.1 (PTFE backbone) and 16.7 (sulfonic side chain)	

[a]The solvent's Hildebrand solubility parameter, and normal boiling point are retrieved from the CRC Handbook of Chemistry and Physics.[31] [b]The Hildebrand solubilities for the Nafion are from Yeo.[28]

CO_2 electrolysis, we used a "like for like" rationale to select acetone and methanol as dispersion solvents that have distinct affinities for the ionomer backbone and sulfonated ionic heads, respectively (Table 1). We focused our study on the short side chain ionomer Aquivion (structure shown in Figure 1a) instead of the long-chain PFSA ionomer Nafion, which is historically widely used in PEM fuel cells and CO_2 electrolysis because PFSA ionomers with shorter side chains are reported to provide better proton conductivity and thermal stability than Nafion.[30,32] Further, Ozden et al.[33] reported that CLs with Aquivion achieved higher partial current densities for CO_2 electrolysis to ethylene than CLs with Nafion. Importantly, acetone and methanol have similar normal boiling points (56 and 65 °C, respectively) and enthalpies of vaporization (31.3

and 35.2 kJ mol^{-1}, respectively),[31] which allows us to minimize the impact of differences in solvent evaporation rates on the ionomer conformation and morphology when drying the CL.

Our study included measuring the mobility of the Aquivion backbone and side chain in solvents, characterizing Aquivion films cast on Cu foils and glassy carbon substrates, and comparing the CL structures and CO_2 electrolysis performance of Cu–Aquivion-coated GDEs in a catholyte-fed flow cell electrolyzer. The Aquivion films and CLs on gas diffusion layers we prepared with acetone inks were more hydrophobic than those prepared with methanol. The acetone-CL GDEs achieved higher selectivity for CO_2 electrolysis to multicarbon (C_{2+}) products at current densities above 200 mA cm^{-2} than did the methanol-CL GDEs. We attribute this result to the acetone-produced more uniform and packed CL structure facilitating higher local CO_2 concentration and local pH values than did the methanol-produced CLs, favoring the formation of C_{2+} products over C_1 products. Our results demonstrate that catalyst inks containing high concentrations of Aquivion promote greater ionomer–ionomer self-interactions and play a role in determining the CL structure and wettability.

2. EXPERIMENTAL SECTION

2.1. Preparation of the Aquivion Film on Cu Foil and a Glassy Carbon Plate. Copper foils (0.5 mm thickness, 99.99% metal basis, Sigma-Aldrich) were polished first with three grades of sandpapers (700, 1500, and 2000) and then to a mirror finish with diamond and alumina polishing kits (ALS-Japan), and then, they were washed with Millipore water (≥18 MΩ cm resistivity) and dried in air. The same procedure was used to polish the glassy carbon plate (CAS 7440-44-0, Alfa Aesar), except without sandpaper. We measured the contact angles of the polished foils and selected only foils within 75 to 90° contact angles for the ionomer film substrates.

We used a series of different concentration ionomer dispersions with 263 μL of Aquivion (25% in water, Sigma-Aldrich) with sufficient acetone (≥99.9%, Sigma-Aldrich) or methanol (≥99.9%, Sigma-Aldrich) to give ionomer concentrations of 1, 10, and 20 g L^{-1}. We sonicated the Aquivion–solvent mixtures for 60 min before drop-casting the mixture directly onto the substrate to achieve 40 μg Aquivion cm^{-2} loadings. The drop-casted samples were dried in the atmosphere for 1 h before further characterization. Our preliminary experiment shows that the film wettability remains constant after 30 min of drying (Figure S1).

2.2. Preparation of the Catalyst Layer on the Gas Diffusion Layer. We used copper nanoparticles (Cu NPs, 25 nm particle size, SKU 774081, Sigma-Aldrich) spray-coated on a commercial gas diffusion layer (GDL 240, Fuel Cell Store) as the cathode GDE for the CO_2 electrolysis tests in a flow cell electrolyzer. We prepared catalyst inks with 100 mg of Cu NPs, 263 μL of Aquivion (25% in water, Sigma-Aldrich), and appropriate volumes of acetone or methanol to match the ionomer concentrations used in the Cu foil experiments (i.e., 1, 10, and 20 g L^{-1}). The catalyst ink was sonicated for 60 min before being spray-coated on the GDL using an airbrush kit (RS components). The CL loading was verified to be 1.3 ± 0.05 mg cm^{-2} of Cu NP + Aquivion on a GDL by measuring the GDE weight difference before and after spray coating. The GDEs were left to dry on a hot plate at 50 °C for at least 30 min before letting the GDEs completely dry in vacuum overnight.

2.3. Material Characterization. *2.3.1. Aquivion Chain Mobility Measurement.* 1 g L^{-1} Aquivion concentration solution in acetone and methanol prepared for Cu foil and glass carbon coating was analyzed with fluorine-19 nuclear magnetic resonance (19F NMR) (Avance-500) by using the method reported by Johnson et al.[34] The fluorine chemical shift of Aquivion in each solvent was labeled based on a previous report in the literature.[35] The following equations were used to calculate the degree of chain mobility from the inverse of the full width of a peak at half-maximum.[22,36]

$$\text{Chain mobility} = \frac{1}{\text{full width of peak at half maximum}} \quad (1)$$

2.3.2. Surface Wettability Measurement. For each sample, 5 ± 0.2 μL of either deionized water or 1 M potassium hydroxide (KOH) was dispensed at a minimum of three locations using a 1–10 μL volume pipet. The contact angle images were captured using a 3 Megapixel CMOS digital camera with a 50 mm Nikon lens and a 12 V light source (detail described in Mahoney et al.).[37] To obtain the contact angles from the captured images, a custom image analysis algorithm was employed, as outlined in the work of Idros and Li.[38] For measuring CLs' wettability after electrolysis, the GDEs were disassembled from the electrolyzer, and the residual electrolytes and salt on the MPL surface were thoroughly rinsed off with deionized water. Subsequently, the rinsed GDEs were dried under atmospheric conditions before subjecting to further characterizations.

2.3.3. Other Characterizations. In-plane resistance measurements were used to characterize electrical resistance of the GDE sheet, which was measured by using the KeithLink four-point probe. The resistance of at least five locations was measured for one sample. Scanning electron microscopy (SEM, JEOL 7100) was used to characterize the CL morphology. X-ray photoelectron spectroscopy (XPS) was performed on a Kratos Axis Ultra with a monochromatic Al Kα (1486.6 eV) radiation source for excitation. The XPS spectra were analyzed with the CASA software. The roughness measurement was performed with a Zeta 300 3D optical profiler with a magnificence of 50× at least reported is the average of three locations of each CL. A Bruker Dimension ICON atomic force microscope was used to image the surfaces of the Aquivion-coated Cu foil and glassy carbon plate. The ScanAsyst mode was utilized with the ScanAsyst-Air probe at a spring constant of 0.4 N m^{-1}. The film thickness was measured through the KLA P7 Stylus profiler with a sensitivity of 10 nm operated with a constant force of 20 mg as the stylus tip was dragged across the film to the substrate surface.

2.4. CO$_2$ Electrolyzer Assembly and Operation. The performances of the Cu NPs + Aquivion-coated GDEs prepared with different catalyst inks were evaluated for CO_2 reduction to C_2 products in a vapor-fed flow cell electrolyzer with the 0.785 cm^2 Cu NP GDE as the cathode; a 6 mm thick nickel foam (99.5%, Goodfellow Cambridge Limited) as the anode; and a Nafion 117 PEM as the separator. The Nafion 117 membrane was immersed in 0.5 M KHCO$_3$ overnight before being used in the electrolyzer. We utilized the Nafion 117 PEM in our electrolyzer to mitigate the crossover of anionic products (e.g., formate) between the catholyte and the anolyte chamber. A Hg/HgO (1 M NaOH, ALS Japan) reference electrode was inserted outside of the electrolyzer, as shown in Figure S2. The potential reported is the cathode potential after the uncompensated resistance. We circulated separate solutions of 1 M KOH at 10 mL min^{-1} as both the catholyte and anolyte. The CO_2 feed was controlled with an MKS mass flow controller at 50 mL min^{-1} to the gas side of the cathode GDE. The electrolyzer effluent gas flow rate (unreacted CO_2 + gas products) was quantified using a flowmeter (Optiflow 520, Sigma-Aldrich, ±3% resolution). We measured the catholyte seepage rate to indicate electrolyte flooding in the cathode using the gravimetric approach that our lab recently reported.[39]

We performed the electrochemical experiments with a Metrohm Autolab PGSTAT302N electrochemical workstation. The gas products from the cathode side of the electrolyzer were analyzed in a Shimadzu Nexis GC-2030 instrument gas chromatograph with a flame ionization detector (FID), a thermal conductivity detector (TCD), and a ShinCarbon packed column (ST 80/100, 2 mm ID, 1/8 OD Silco, Restek). The first gas sample was analyzed after 10 min of chronovoltammetry. A new GDE was used at each current supplied and underwent 1 h of electrolysis. Three gas injections were performed at 16 min intervals, and the average value was reported. Simultaneously, the electrolyzer's overall potential was recorded through a digital multimeter, displayed in Figure S3.

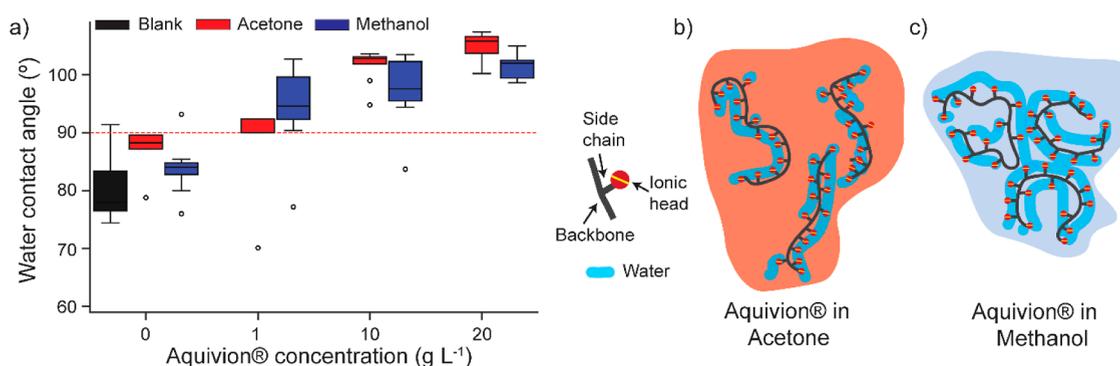The Faradaic efficiencies for the gas products were calculated through

Figure 2. Comparing Aquivion film wettability and potential conformation in acetone and methanol. (a) Initial wetting contact angle of polished blank Cu foil and Cu foils coated with dried Aquivion film prepared by casting different concentrations of Aquivion in acetone and methanol. The Aquivion loading on the Cu foils is kept consistent except for the Cu foil with an Aquivion concentration of 0 g L^{-1}. The length of the box plots represents the lower and upper quartiles of the contact angle median, while the empty circles indicate the outlier of the measured data. We made nine contact angle measurements for each sample on three different areas of three independently prepared foils. (b,c) Schematic illustration of a 2D slide of Aquivion molecules' potential conformations in the acetone and methanol dispersion solvent, with each Aquivion sulfonated ionic head side chain and fluorinated backbone orientation representing their potential interaction with the solvent.

$$FE_i = \frac{P \times v \times c_i \times F \times N_i}{R \times T \times j} \times 100\% \quad (2)$$

where P is the operating pressure of 101.31 kPa, F is the Faraday constant (96,484 C mol^{-1}), R is the gas constant (8.31446 J K^{-1} mol^{-1}), v is the effluent gas flow rate (mL s^{-1}), c_i is the gas product species i concentration measured from the gas chromatography (mol s^{-1}), N_i is the number of electron transfers required to produce 1 mol of the gas product i, T is the reactor temperature (K), and j is the total current density (mA cm^{-2}) calculated from the current applied by the PGSTAT302N and the cathode's geometric surface area (0.785 cm^2).

^{1}H NMR (Bruker Avance 500 high-resolution NMR) was used to analyze the liquid products. The catholyte effluent was collected after 1000 s of the CO$_2$ reduction reaction (CO$_2$RR). 400 μL of the effluent was mixed with 200 μL of heavy water [containing 0.05 vol % dimethyl sulfoxide (DMSO, anhydrous, ≥99.99%, Sigma-Aldrich) in deuterium (D$_2$O, 99.9 atom % D, Sigma-Aldrich)]. The DMSO in D$_2$O acts as the internal reference for the NMR calculation. The average Faradaic efficiency for the liquid products over the time period of an experiment was calculated by

$$FE_i = \frac{v_{catholyte} \times c_i \times F \times N_i}{j} \times 100\% \quad (3)$$

where c_i is the concentration of the liquid product determined from the NMR analysis (mol) and $v_{catholyte}$ is the volume of the catholyte during the test period (300 mL).

We corrected the measured cathode potential (E) to the reversible hydrogen electrode (RHE) scale using the Nernst equation

$$E_{RHE} = E + E_0 + \frac{2.303 \times R \times T}{F} \times pH + (Ru)J \quad (4)$$

where E_0 is the standard reference potential (0.118 V for the Hg/HgO reference electrode), pH is the catholyte pH value, Ru is the uncompensated resistance (ohm), and J is the total current applied.

3. RESULTS AND DISCUSSION

3.1. Solvent and Ionomer Interaction. We tested the hypothesis that solubility parameters affect the mobility of the Aquivion side and backbone chains in methanol and acetone using the 19-fluorine (^{19}F) NMR spectroscopy method reported by Johnston et al.[34] The NMR spectra (Figure 1b) of 1 g L^{-1} Aquivion in each solvent exhibit peaks at 78, 117, and 137 ppm attributed to the fluorine in the sulfonated ionic head side chains and a peak at 121 ppm attributed to fluorinated carbons in the polymer backbone.[35] Based on

Figure 1b, the relative mobility of Aquivion's side chain and backbone in each solvent can be determined based on the inverse of the full width of the peak at half-maximum.[30,34,36,40] The Aquivion side chain relative mobilities in acetone (5.3 kHz^{-1}) and methanol (5.2 kHz^{-1}) are similar, suggesting similar solvation of PFSA side chains in the two solvents. In contrast, the mobility of the backbone is two times greater in acetone (2.3 kHz^{-1}) than in methanol (1.1 kHz^{-1}), and these properties indicate that acetone tends to solvate the Aquivion backbone more than methanol does. The enhanced solvation of the Aquivion backbone in acetone will increase the phase separation, resulting in smaller and loosely coiled aggregates of the ionomer when deposited on a surface, and weaker solvation of the backbone in methanol is expected to lead to secondary ionomer aggregations with larger rod and tube-like structures.[29,30,41]

Before conducting experiments with the complex structure of Cu NP catalysts deposited on porous GDEs, we coated Aquivion on polished Cu foils and glassy carbon substrates as simplified models to mimic Aquivion coating behavior on Cu NPs[42] and to study the morphology, surface chemistry, and wettability of Aquivion films prepared from dispersions in acetone and methanol. We drop cast the Aquivion films onto the substrates from dispersions of 20 g of Aquivion in 1 L of acetone or methanol and then dried the film at room temperature for 1 h to achieve ionomer loadings of 40 μg cm^{-2}. In these experiments, we opted to control the ionomer mass loading rather than film thickness as mass loading is the parameter more easily controlled in spray-coating preparation of the CL on the GDE. Figure 1c–e shows the roughness of Aquivion films on Cu foils determined by atomic force microscopy (AFM). The Aquivion films cast from acetone dispersions produced a more continuous and flatter structure than those from the methanol dispersion. Our observation, consistent with other reports,[23,24] is that dispersions in solvents with a lower solubility parameter produce more uniform ionomer films than films prepared from a solvent with a higher solubility parameter.

During the casting process, the Aquivion−solvent mixture spreads and pins to the Cu foil surface, forming solid residues in a ring-like pattern along the contact line,[43,44] known as the coffee stain effect, refer to Figure S4. The film cast with

acetone exhibits a more pronounced coffee stain effect, as evidenced by the peak height at the film edges measuring 2.06 $\pm$ 0.01 μm before plateauing to an average of 0.67 $\pm$ 0.09 μm at 500 μm from the edges. In contrast, the film cast with methanol exhibits minor variations in height at the edges compared to the overall film pattern, but it still displays nonuniformity, as seen by the drop in film height at around 500 μm from the edges. In general, acetone and methanol-cast Aquivion films have thicknesses exceeding 200 nm, indicating an isotropic molecular orientation of the ionomer nano-domains, where the ionomer backbone and side chains align isotropically with the substrates.[45,46] However, it is important to note that both films exhibit some degree of nonuniform ionomer distribution across the film. Therefore, accurately determining and reporting the film thickness might result in overestimating its value.

An apparent artifact in the AFM images in Figure 1c−e is the scratch defects created by polishing Cu foils, a standard practice in preparing foil electrodes. To check that these scratches do not significantly affect the conformation of the ionomer films, we performed the same Aquivion film casting experiments on glassy carbon substrates (surface roughness results in Figure S5) and observed similar trends to the films cast on the Cu foils, with the Aquivion film cast with methanol consistently rougher than the Aquivion film prepared with acetone (Figure S6). These control experiments helped rule out the potential impacts from the substrates and highlight the solvent's role in controlling the conformation of Aquivion in the film.

3.2. Effects of Solvents on Ionomer Surface Wettability.

As the solvents in the ionomer dispersion influence the ionomer aggregation in the film, we expect that the choice of the solvent will affect the wettability of both pure Aquivion films and the CLs prepared with the ionomer−solvent mixture, ultimately impacting the CO_2RR performance.[13,30,47,48] Figure 2a compares the contact angles of water droplets on Aquivion film-coated Cu foils measured. In Figure 2a, the blank (black) data show contact angles measured on polished Cu foils that were not washed in either solvent, and 0 g L^{-1} ionomer concentration data are control experiments for contact angles measured on polished Cu foils that were washed in acetone (red) and methanol (blue). We observed a wide variation of contact angles in nine measurements on unwashed polished Cu foils (three regions on three independent foils). After washing the polished Cu foils in acetone or methanol, the range of contact angles observed was narrowed but still within the uncertainty range of the contact angles on the unwashed, polished Cu foil (contact angle 76.4° $\pm$ 8.5°). This contact angle result, together with the XPS analysis of the Cu foils in Figure S7, provides evidence that washing in acetone or methanol does not significantly affect the surface chemistry or structure of the Cu substrate.

One of our experimental protocols to reduce the effect of Cu foil artifacts on the interpretation of Aquivion film contact angle measurements was to only select polished Cu foils with similar mean contact angles for drop casting the Aquivion film. For Cu foil with Aquivion films, the contact angles of the water droplet on Aquivion-coated Cu foils showed that the surface became more hydrophobic. The contact angle increased by 36° for acetone and 18° for methanol when the concentrations of Aquivion in the dispersion were increased from 1 to 20 g L^{-1}. We repeated these measurements with 1M KOH droplet, the electrolyte used in the CO_2 electrolysis tests, and observed

trends similar to those of the water contact angles (Figure S8). The increased hydrophobicity of the Aquivion films from higher concentration dispersions is likely related to the greater exposure of the fluorinated backbones by acetone and the enhanced primary aggregation of the backbones in the higher concentration solutions.[45]

Also, to verify that our hypothesis tests for the role of solvents on ionomer wettability are not significantly affected by polishing scratches on the Cu foils, we repeated the film casting and contact angle measurements for Aquivion films on glassy carbon plates. A clean glassy carbon plate is less hydrophobic (47.5° $\pm$ 4.8°, Figure S9) and is smoother (Figure S6 shows that the R_q glass carbon plate is approximately one-third of the R_q of Cu foils). When the Aquivion film is cast on the glassy carbon surface, the hydrophobicity of the Aquivion film is notably higher when prepared with acetone than with methanol. The increase in hydrophobicity of the ionomer films prepared from acetone over glassy carbon and Cu foil surfaces can primarily be attributed to the film's wettability rather than only scratch defects of substrate surfaces.

The comparison of the wettability of films on Cu foils and glassy carbon also shows that the substrate type influences the extent of the solvent impact on the ionomer film wettability. When cast on a hydrophilic glassy carbon plate, the ionomer molecules are more likely to form isotropic structures, the conformation of Aquivion side chains extending inward in the film prepared with acetone and outward in the film prepared with methanol.[46,48−51] A similar ionomer structure can be anticipated when deposited on the Cu foil surface, and despite absolute differences in contact angles of the ionomer films observed on Cu and glassy carbon, these findings confirm that the acetone solvent induces a more hydrophobic ionomer film than methanol. However, the bumps on the rougher Cu foil surface partially mitigate the effects of solvent interactions because the film's wetting state on the Cu foil may adopt either the Wenzel or Cassie−Baxter state, in which surface roughness amplifies the surface hydrophobicity.[52]

Notably, the film prepared from a lower concentration (1 g L^{-1}) of Aquivion in acetone produces smaller Aquivion aggregates than the film prepared from Aquivion in methanol (Figure S10), resulting in the contact angle measured for the Aquivion film prepared from the diluted acetone dispersion representing the mixed wettability of the ionomer film and Cu foil.

We examined the surface chemistry of the Aquivion films cast on the Cu foils using XPS to understand the conformation of the sulfonated side chains and the fluorinated backbones (Figure S7). Figure S12 shows the concentration intensity ratio I_F/I_S of the F 1s, predominantly in the fluorinated backbone, and S 2p in the sulfonic side chains of the dried Aquivion films. Despite the total Aquivion loadings on Cu substrates being the same in each test, at each of the three dispersion concentrations, the I_F/I_S ratio of Aquivion films from the acetone dispersion is slightly higher than the I_F/I_S ratio of Aquivion films prepared from methanol dispersions. Even though the I_F/I_S ratios of the Aquivion films prepared with acetone and methanol show a minor difference, the consistently higher F 1s signal over S 2p signals for the ionomer film cast from acetone indicates that the observed ionomer wettability variation from different solvents is related to the conformation of the ionomer molecules in the films.

Aquivion molecules are more likely to unfold and arrange with the fluorine backbone pointing outward in acetone (as illustrated in Figure 2b) than in methanol (Figure 2c).[22,29,30,41,50] Thus, the film cast from acetone ink spreads more evenly with smaller Aquivion aggregates and is hydrophobic across the substrates than the film cast from methanol dispersions. Lee et al. describe this type of ionomer conformation that we observed from acetone inks as the primary aggregation of the ionomer.[25] In contrast, the weaker solvation and lower mobility of the backbone in methanol lead to an increase in ionic aggregation between the primary aggregated Aquivion molecules. The ionic aggregation is due to the ionomer's sulfonic heads' electrostatic interaction being greater, outweighing the ionomer's mobility in methanol dispersion.[25,50] Consequently, the Aquivion film cast from a methanol ink features a film with lower hydrophobicity with large and discontinuous aggregations.[22,29,30,41]

3.3. Effects of the Solvents on the Formation of Catalyst Layers on GDEs.

The previous section identified the influence of solvents on the morphology, chemistry, and wettability of Aquivion films on flat surfaces (Cu foils and glassy carbon). Next, we use these findings to understand better how solvent choice impacts the properties of the CL deposited on a porous gas diffusion layer. The approach now deals with systems of higher complexities, from ionomer–solvent dispersion to catalyst inks that include Cu NPs and subsequently to porous CL structures deposited on three-dimensional GDLs.

3.3.1. Catalyst Layer Structures. We compared the structures of Cu NPs CLs deposited on a commercial gas diffusion layer (GDL240, Fuel Cell Store) by spray coating catalyst inks with Cu NPs with Aquivion of concentrations 1 and 20 g L^{-1} in acetone and methanol. The catalyst-to-ionomer weight ratio in each ink and the total catalyst plus ionomer loadings were constant (1.3 ± 0.05 mg cm^{-2} of Cu NP + Aquivion on a GDL). The Aquivion loadings in the CLs at both concentrations were the same. Consistent with our observations of the ionomer films on flat surfaces, the dilute catalyst ink (1 g L^{-1} Aquivion in solvent) produced a more evenly distributed CL than the 20 g L^{-1} ink for both solvents (Figure 3). The discontinuous CLs formed using the 20 g L^{-1} Aquivion ink are likely due to a higher frequency of ionomer–ionomer interactions leading to larger primary backbone aggregations. Interestingly, the CLs prepared with acetone (acetone-CLs) still have a more continuous structure than those prepared with methanol (methanol-CLs), even in the CL prepared with concentrated ionomer inks. Figure S13 shows the average roughness of the catalyst on the GDE, measured with an optical profiler. As the Aquivion concentration in ink increases from 1 to 20 g L^{-1}, acetone-CL's roughness increases from 1.5 ± 0.17 to 3.4 ± 0.19 μm, while methanol-CL's roughness increases from 2.0 ± 0.26 to 4.3 ± 0.63 μm. In either case, acetone-CL still has lower roughness than methanol-CL.

Across both concentrations, acetone-CL consistently exhibited a thinner CL than methanol-CL, as shown from the CL cross-section SEM images in Figure S14. For example, at a concentration of 20 g L^{-1} Aquivion, acetone-CL is 24% thinner than methanol-CL. Hence, the acetone-CL is denser and has higher internal connectivity with smaller Aquivion aggregations within the CL than methanol-CL. However, at a lower Aquivion concentration of 1 g L^{-1}, both CLs showed an increase in CL thickness: 47.8 ± 2.9 μm for acetone-CL and
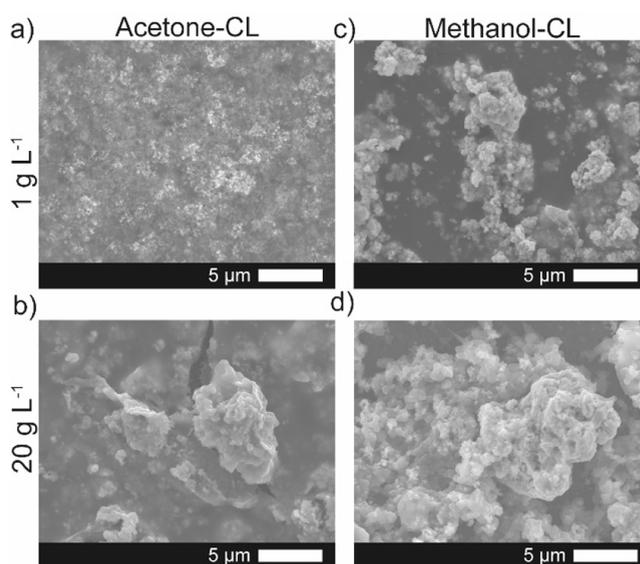

Figure 3. Microstructure of the copper NPs with Aquivion CL on the GDL240 gas diffusion layer (GDL). SEM images of the prepared CL surface by spraying a mixture of copper NPs (average particle size: 25 nm TEM) with Aquivion at concentrations (a) 1 or (b) 20 g L^{-1} in acetone. Follows with the SEM images of the surface of copper and Aquivion CL prepared by spraying a mixture of copper NPs with Aquivion at (c) 1 or (d) 20 g L^{-1} in methanol.

54.8 ± 5.8 μm for methanol-CL. As the ionomer is a binder to immobilize catalyst particles in the CL, its conformation is essential in determining the CL structure and its impact on the CO$_2$RR performance.

3.3.2. CO$_2$ Electrolysis Performance. To measure the electrochemical performance of acetone-CL and methanol-CL prepared with 20 g L^{-1} Aquivion concentration, we performed CO$_2$ electrolysis in a flow electrolyzer with 1 M KOH recirculating as the anolyte and catholyte (separately). The full electrochemical test procedure, accompanied by the electrolyzer's overall potential, is described in the Experimental Section. Figure 4a,b consistently illustrates that the cathodic potential required for acetone-CL is more negative than that for methanol-CL as current densities increase. When we measured the sheet resistance through a four-point probe to further investigate the electrical resistance inherent in the CL, we found that acetone-CL exhibited six times higher electrical resistance than methanol-CL, a trend consistent with the potential observed in the CLs (Figure S15). Our observation of methanol-CL's low overpotential is consistent with Ramya et al.'s findings, where introducing a solvent with a solubility parameter close to the ionic head reduces the polymer resistance, thereby improving the conductivity.[53] Both CLs have similar catalyst and ionomer loadings, suggesting that the continuous ionomer backbones on the CL are the probable reason for the high electrical resistance observed in the acetone-CL, which will hinder the distribution of electrons on the catalyst surface.

For all current densities in these experiments, ethylene (C$_2$H$_4$) was the primary product for both CLs. The liquid products for both CLs are primarily formate and ethanol with small amounts of acetate and propanol. Only acetone-CL produces propanol at high current densities, possibly due to an enhancement in the CO dimerization on the catalyst surface. The ethylene selectivity peaks at 300 mA cm^{-2} in both CLs,
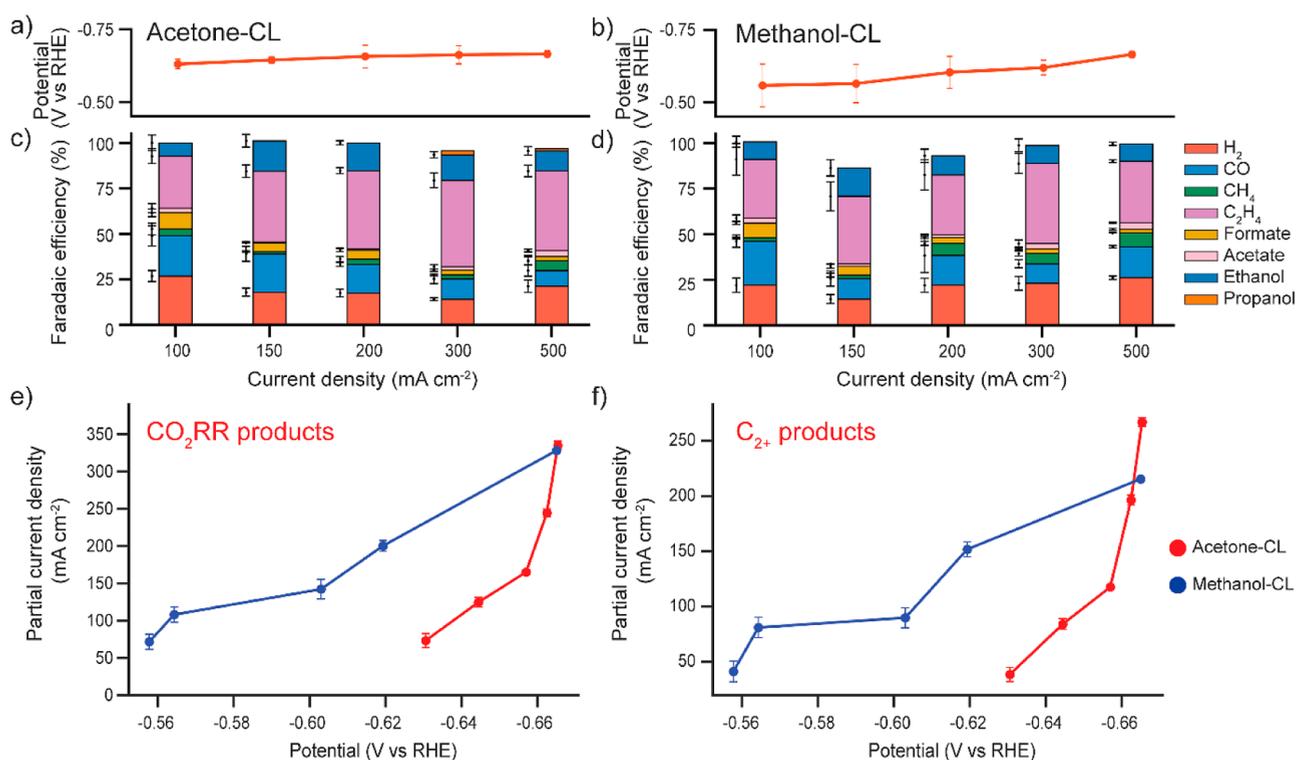
Figure 4. Comparison of the CO_2 electrolysis performance for the CL prepared with acetone (acetone-CL) and methanol (methanol-CL) at an Aquivion concentration of 20 g L^{-1} in a continuous flow electrolyzer. The average cathode potential of (a) acetone-CL and (b) methanol-CL at current densities of 100−500 mA cm^{-2} in the flow electrolyzer. The average Faradaic efficiency (FE) of the detectable gas and liquid products measured through gas chromatography and NMR for (c) acetone-CL and (d) methanol-CL at current densities of 100−500 mA cm^{-2}. The average partial current densities of (e) all CO_2 electrolysis products and (f) C_{2+} products (C_2H_4, acetate, ethanol, and propanol) at potentials of −0.54 to −0.68 V vs RHE. The error bars in (a−f) represent the standard deviation of nine measurements of CO_2 electrolysis performance from three measurements of three replicate 1 h CO_2 electrolysis on the CL.

with values of 47.4 ± 4.0% for acetone-CL and 37.6 ± 5.5% for methanol-CL (Figure 4c,d). At high current densities, acetone-CL exhibited a selectivity of C_{2+} over single carbon (C_1) products that was higher than that of methanol-CL (Figure S16). For instance, at 500 mA cm^{-2}, the acetone-CL selectivity of C_{2+} over C_1 products is 2.05 times that of methanol-CL, and ethylene selectivity remained at 37.9 ± 3.2% for acetone-CL but fell to 29.4 ± 0.7% for methanol-CL. As for the CO_2RR partial current densities, these values are drastically different for acetone-CL and methanol-CL, revealing the kinetic characteristics of the CLs. Figure 4e,f illustrates a more significant increment of the CO_2RR and C_{2+} production rate on acetone-CL than on methanol-CL with an increase in potential. This difference is most apparent at the −0.66 V vs RHE cathode potential, where the CO_2RR and C_{2+} partial current densities over acetone-CL start to outperform the methanol-CL.

Figure S17 displays the overpotential and gas product selectivities with time for the acetone-CLs and methanol-CLs. Acetone-CL and methanol-CL display stable overpotential over the 1 h test, which allows comparisons in this test duration. Acetone-CL displays relatively stable product selectivities for all of the gas products produced. In contrast, methanol-CL illustrates a fluctuation in ethylene production and a decrease in the selectivity for CO and CH_4 over time. This difference is due to the uneven distribution of the CL, and poor connectivity resulting from the thick methanol-CL can lead to variation in the local reaction and hinder the efficient

and uniform distribution of CO_2 and electrons at the catalyst surface.

We compared the CLs' properties before and after electrolysis to further verify the impact of the catalyst ink dispersion solvents on the stability of the CL surface wettability. Before electrolysis, acetone-CL and methanol-CL prepared with 20 g L^{-1} Aquivion inks show similar wetting contact angles ranging from 131 to 136°. After 1 h of electrolysis at 200 mA cm^{-2}, both CLs experienced a drop in hydrophobicity (Figure S18). Methanol-CL shows a more significant loss in hydrophobicity than acetone-CL, which was also evidenced by the larger change in methanol-CL's double-layer capacitance from 1.3 ± 0.04 to 360.0 ± 14.5 mF than the double-layer capacitance increment in acetone-CL from 0.6 ± 0.01 to 55.8 ± 2.3 mF (Figure S19). Measuring the double-layer capacitance of CLs provides insights into the areas of the electrode that is wetted and accessible to the electrolyte. Therefore, the sharp increase in capacitance experienced in methanol-CL signifies a substantial increase in electrolyte invasion within the CL pores, leading to sluggish CO_2 transfer and unstable CO_2 electrolysis performance, as illustrated in Figure S17.

Furthermore, when comparing the CL structure after electrolysis (Figure S20), we found that both CLs exhibit a discernible change in the CL structure, where more copper particles were exposed to the electrolyte during electrolysis.[54] The uneven CL and reduced Aquivion coverage in methanol-CL amplify such a CL structure change, which might increase the electrolyte accessibility within the CL. We measured the
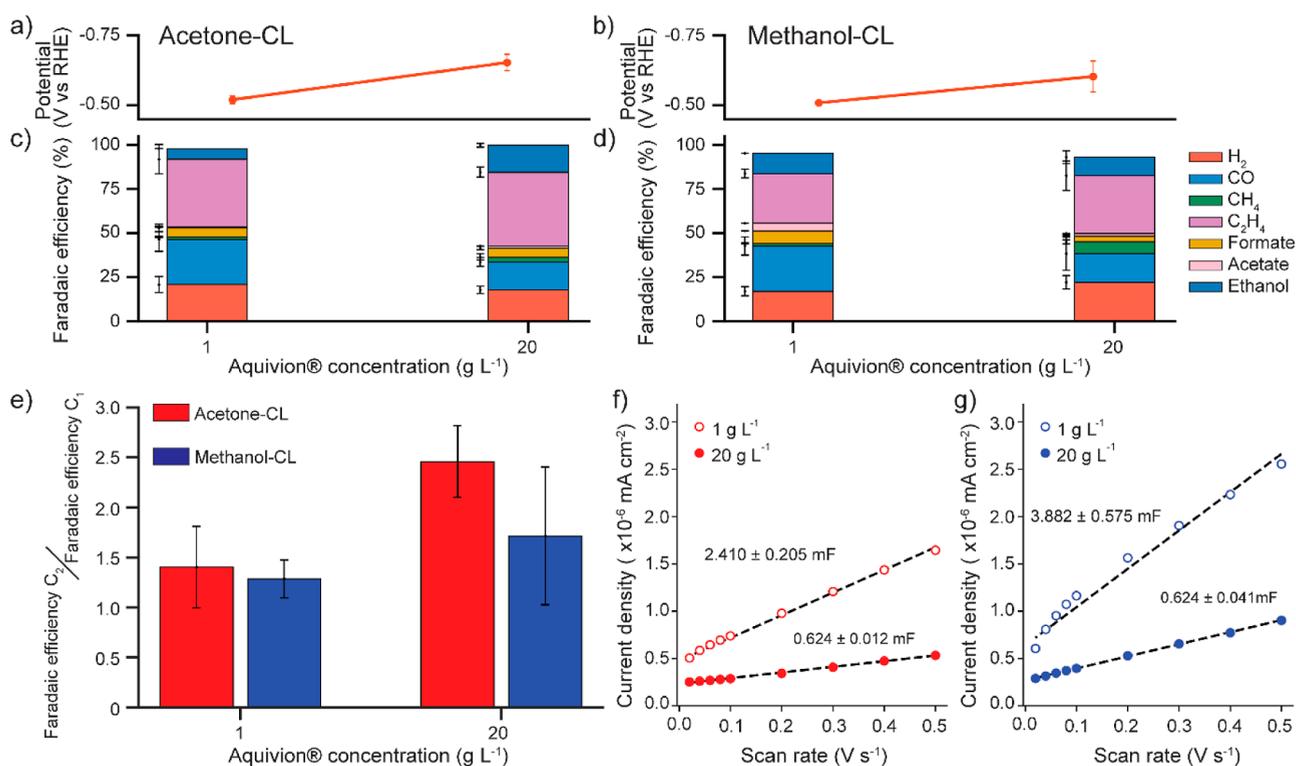
Figure 5. Comparison of the CO_2 electrolysis performance at 200 mA cm^{-2} for the CL prepared with acetone (acetone-CL) and the CL prepared with methanol (methanol-CL) with Aquivion concentrations of 1 and 20 g L^{-1}, in a continuous flow electrolyzer. Average cathode potential of (a) acetone-CL and (b) methanol-CL with an Aquivion concentration of 1 and 20 g L^{-1} at 200 mA cm^{-2}. Average Faradaic efficiency (FE) of the detectable gas and liquid products measured through gas chromatography and NMR for (c) acetone-CL and (d) methanol-CL with Aquivion concentrations of 1 and 20 g L^{-1} at 200 mA cm^{-2}. (e) Ratio of C_2 products over C_1 products (CO, CH_4, and formate) for acetone-CL and methanol-CL with concentrations 1 and 20 g L^{-1} at 200 mA cm^{-2}. Comparing the capacitive current as a function of the scan rate in 1 M $KHCO_3$ within the open circuit potential range for the copper CL prepared with 1 and 20 g L^{-1} Aquivion concentrations in (f) acetone-CL and (g) methanol-CL. The copper CLs' specific double-layer capacitance (C_{dl}) values are calculated from the capacitive current slope. The C_{dl} displayed in parts (f,g) is the average of three independent capacitive measurements on each CL. The error bars in (a−e) represent the standard deviation of nine measurements of CO_2 electrolysis performance from three measurements of three replicate 1 h CO_2 electrolysis on the CL.

electrolyte seepage rates from the GDEs during operation[39,55] to understand further the wetting in each CL. We found that acetone-CL exhibited no detectable seepage rate at all current densities. In contrast, the methanol-CL prepared with 20 g L^{-1} Aquivion ink showed a high seepage rate of 12 mg min^{-1} from current densities of 300 mA cm^{-2}. Therefore, we can safely conclude that the acetone-CL has a more stable CL hydrophobicity during the CO_2RR and improves electrode stability selectivity at high current densities. This result is consistent with the wetting behavior of the ionomer films on flat substrates (Figure 2a). The ionomer cast from acetone is more hydrophobic, preventing the electrolyte from intruding into the GDE pores.

We also compared the CO_2RR performance at 200 mA cm^{-2} over electrodes prepared from catalyst inks with 1 and 20 g L^{-1} Aquivion in acetone and methanol. We observed higher overpotentials for the CLs prepared from 20 g L^{-1} (Figure 5a,b), likely due to the high Ohmic loss caused by the discontinuous CL coverage on the GDLs (Figures 3 and S13). Additionally, acetone-CL exhibited a significant increase in the in-plane resistance compared to methanol-CL at higher Aquivion concentrations in ink (Figure S15). This result suggests that the Aquivion backbone in the acetone-CL swelled more than the ionomer in the methanol-CL, resulting in greater hydrophobicity and limited electron transfer.

The selectivity toward C_{2+} products over C_1 products increases with the Aquivion concentration in the catalysts ink by 76 and 34% for CLs made with acetone and methanol, respectively (Figure 5e). We believe that the significant selectivity improvement by acetone arose from the Aquivion conformation and wettability exhibited in acetone. As shown in Figure 3, the deposited CL shows a more continuous layer in acetone than in methanol, regardless of the Aquivion concentrations in the catalyst ink.

Despite acetone-CL and methanol-CL showing similar contact angles at each concentration, as shown in Figure S21, acetone-CLs consistently show lower double-layer capacitance than methanol-CL (Figure 5f,g). As we prepared the CLs with the same catalyst loadings, we anticipated the physical surface areas of the CLs to be similar. In this case, the measured double-layer capacitance is primarily a function of the CL wetting behavior: a large capacitance indicates a large wetted catalyst area. The lower double-layer capacitance exhibited by the acetone-CL is consistent with the denser morphology of the acetone-CL observed by SEM and one factor that explains the lower rate of flowing in acetone-CL.

Moreover, a decrease in Aquivion concentration leads to a drop in hydrophobicity for both CLs and increases the CLs' double-layer capacitance. It can be inferred that the CL prepared with lower Aquivion concentration inks leads to better surface wetting. In contrast, CLs from high Aquivion

concentration inks impede the electrolyte from wetting the surface. The reduced hydrophobicity in diluted Aquivion cases could be attributed to the reduced roughness of the CLs (Figures S13 and S14).

CO_2 electrolysis over Cu electrocatalysts is highly sensitive to the local reaction environment, such as CO_2 local availability and local pH. In particular, C_{2+} products are favored at high local pH and *CO surface coverage in the CL.[56] First, the ionomer deposited from acetone has a higher hydrophobicity, which limits the availability of water molecules within the CLs, evidenced by acetone-CL's lower double-layer capacitance after electrolysis than that of methanol-CL. As a result, the limited water molecules within the acetone-CLs cause an increase in the local pH (Figure 6). Because C_{2+}
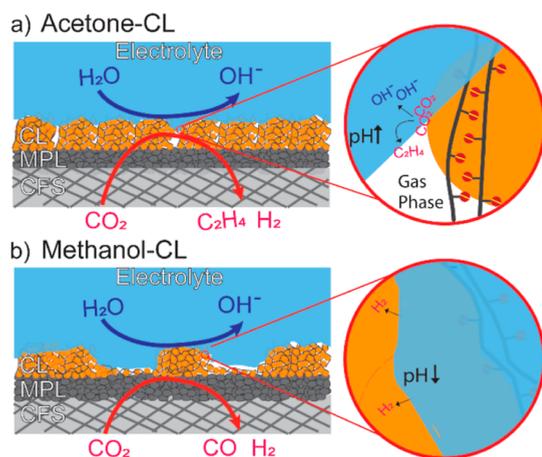

Figure 6. Schematic illustration of CO_2 electrolysis at the CL prepared with acetone (acetone-CL) and methanol (methanol-CL). (a) CO_2 electrolysis on a uniform and greater Aquivion film hydrophobicity of acetone-CL, which potentially has more triple-phase boundaries within the CL and a higher local pH to promote the formation of C_{2+} products. (b) The CO_2 electrolysis on a nonuniform and lower Aquivion film hydrophobicity of methanol-CL has limited triple-phase boundaries and lower local pH due to submerging of the electrolyte at the CL surface.

products are independent of local pH, a high local pH can shift the potential to a more positive value vs RHE by an approximately $0.059\times$ pH increase. The hydrophobicity of the ionomer from acetone could partially contribute to the enhancement of C_{2+} production rates, particularly at current densities above 200 mA cm^{-2}. The high local pH at the acetone-CL can also explain the suppression of the HER and CO_2RR to methane (Figures 4c,d and S22).[27,57] However, operating with high local pH can result in a high loss of CO_2 into the electrolyte to form carbonates,[58] which we calculated to be happening more in acetone-CL than methanol-CL at high current densities (Figure S23).

Second, the local CO_2 availability can dramatically influence C_{2+} selectivity because C_{2+} production proceeds via a second-order reaction of the *CO surface coverage.[3] The *CO surface coverage is directly related to the CO_2 local availability, which relies on the CO_2 transport across the CL.[19,59] Therefore, the high hydrophobicity and dense structure of acetone-CL, which has the Aquivion backbones exposed, can promote the formation of triple-phase boundaries inside the CL, limit electrolyte accessibility, and shorten the length of CO_2 gas diffusion pathways (Figure 6). Considering the absence of the

apparent seepage rate in acetone-CL across all current densities, as opposed to that in methanol-CL, we infer that the CO_2 transfer in acetone-CL remained unhampered or minimally hampered compared to that in methanol-CL. As a result, a higher C_{2+} products selectivity observed for the CO_2RR with acetone-CL (up to $65.5 \pm 4.5\%$) compared to that with methanol-CL ($50.6 \pm 6.7\%$) at 300 mA cm^{-2} is evidence of the enhancement of CO_2 transport in the acetone-CL experiment.[56]

4. CONCLUSIONS

Our work elucidates the role of dispersion solvents in determining the CL structures for CO_2 electrolysis at high current densities. We identified the dispersion solvents' different solvation capabilities toward the ionomer backbones and ionic heads. Acetone tends to interact more strongly with the fluorinated backbones of the Aquivion ionomer than methanol. As a result, the ionomer deposited from acetone forms a more continuous film with a greater hydrophobicity than its methanol counterparts. Our findings also translate to the deposition of the CL on GDEs: acetone-CL exhibits a more continuous and hydrophobic layer than methanol-CL.

Consequently, the acetone-CLs show improved Faradaic efficiencies for CO_2 electrolysis to C_{2+} products, limiting current densities and resistances against electrode flooding, compared to methanol-CL, particularly at high current densities up to 300 mA cm^{-2}. With methanol-CL susceptible to high electrolyte penetration, it will render a high local water content and sluggish CO_2 transfer to the catalyst surface. Our systematic approach to studying acetone and methanol dispersion solvents in controlling the CL wettability and performance demonstrates an alternative strategy to advance industrially relevant CO_2 electrolysis by manipulating the catalyst ink's dispersion solvents for the catalyst preparation.

Credit authorship contribution statement: **Mohamed Nazmi Idros:** investigation, conceptualization, methodology, software, validation, visualization, formal analysis, and writing—original draft. **Yuming Wu:** investigation. **Timothy Duignan:** conceptualization, supervision, and writing—review and editing. **Mengran Li:** conceptualization, methodology, supervision, and writing—review and editing. **Hayden Cartmill:** investigation. **Irving Maglaya:** investigation. **Thomas Burdyny:** writing—review and editing. **Geoff Wang:** conceptualization, funding acquisition, and supervision. **Thomas E. Rufford:** conceptualization, funding acquisition, project administration, supervision, and writing—review and editing.

■ ASSOCIATED CONTENT

ⓈSupporting Information

The Supporting Information is available free of charge at https://pubs.acs.org/doi/10.1021/acsami.3c11096.

> Schematic of the electrolyzer and CO_2 electrolysis setup; water contact angle images; and additional measurements, including Aquivion film structure and properties measured through KLA and AFM, XPS, CL thickness, roughness, IES, and sheet resistance measurements, and additional CO_2RR performance test results (PDF)

■ AUTHOR INFORMATION

Corresponding Authors

Thomas E. Rufford − *School of Chemical Engineering, The University of Queensland, St Lucia 4072, Australia;*

orcid.org/0000-0002-8865-7976; Email: t.rufford@uq.edu.au

Mengran Li − *Materials for Energy Conversion and Storage (MECS), Department of Chemical Engineering, Faculty of Applied Sciences, Delft University of Technology, 2629 HZ Delft, The Netherlands;* Present Address: Department of Chemical Engineering, The University of Melbourne, Victoria, Australia.; ● orcid.org/0000-0001-7858-0533; Email: aaron.li1@unimelb.edu.au

Authors

Mohamed Nazmi Idros − *School of Chemical Engineering, The University of Queensland, St Lucia 4072, Australia*

Yuming Wu − *School of Chemical Engineering, The University of Queensland, St Lucia 4072, Australia;* ● orcid.org/0000-0003-2809-0338

Timothy Duignan − *School of Chemical Engineering, The University of Queensland, St Lucia 4072, Australia;* Present Address: Queensland Micro- and Nanotechnology Centre, Griffith University, Nathan 4011, Australia; ● orcid.org/0000-0003-3772-8057

Hayden Cartmill − *School of Chemical Engineering, The University of Queensland, St Lucia 4072, Australia*

Irving Maglaya − *School of Chemical Engineering, The University of Queensland, St Lucia 4072, Australia*

Thomas Burdyny − *Materials for Energy Conversion and Storage (MECS), Department of Chemical Engineering, Faculty of Applied Sciences, Delft University of Technology, 2629 HZ Delft, The Netherlands;* ● orcid.org/0000-0001-8057-9558

Geoff Wang − *School of Chemical Engineering, The University of Queensland, St Lucia 4072, Australia*

Complete contact information is available at:
https://pubs.acs.org/10.1021/acsami.3c11096

Notes

The authors declare no competing financial interest.

■ REFERENCES

(1) De Luna, P.; Hahn, C.; Higgins, D.; Jaffer, S. A.; Jaramillo, T. F.; Sargent, E. H. What Would It Take for Renewably Powered Electrosynthesis to Displace Petrochemical Processes? *Science* **2019**, *364* (6438), No. eaav3506.

(2) Jouny, M.; Luc, W.; Jiao, F. General Techno-Economic Analysis of CO₂ Electrolysis Systems. *Ind. Eng. Chem. Res.* **2018**, *57* (6), 2165−2177.

(3) Nitopi, S.; Bertheussen, E.; Scott, S. B.; Liu, X.; Engstfeld, A. K.; Horch, S.; Seger, B.; Stephens, I. E. L.; Chan, K.; Hahn, C.; Nørskov, J. K.; Jaramillo, T. F.; Chorkendorff, I. Progress and Perspectives of Electrochemical CO₂ Reduction on Copper in Aqueous Electrolyte. *Chem. Rev.* **2019**, *119* (12), 7610−7672.

(4) Verma, S.; Kim, B.; Jhong, H.-R. M.; Ma, S.; Kenis, P. J. A. A Gross-Margin Model for Defining Technoeconomic Benchmarks in the Electroreduction of CO₂. *ChemSusChem* **2016**, *9* (15), 1972−1979.

(5) Whipple, D. T.; Kenis, P. J. A. Prospects of CO₂ Utilization via Direct Heterogeneous Electrochemical Reduction. *J. Phys. Chem. Lett.* **2010**, *1* (24), 3451−3458.

(6) Hori, Y.; Wakebe, H.; Tsukamoto, T.; Koga, O. Electrocatalytic Process of CO Selectivity in Electrochemical Reduction of CO₂ at Metal Electrodes in Aqueous Media. *Electrochim. Acta* **1994**, *39* (11−12), 1833−1839.

(7) Xing, Z.; Hu, L.; Ripatti, D. S.; Hu, X.; Feng, X. Enhancing Carbon Dioxide Gas-Diffusion Electrolysis by Creating a Hydrophobic Catalyst Microenvironment. *Nat. Commun.* **2021**, *12* (1), 136.

(8) García de Arquer, F. P.; Dinh, C.-T.; Ozden, A.; Wicks, J.; McCallum, C.; Kirmani, A. R.; Nam, D.-H.; Gabardo, C.; Seifitokaldani, A.; Wang, X.; Li, Y. C.; Li, F.; Edwards, J.; Richter, L. J.; Thorpe, S. J.; Sinton, D.; Sargent, E. H. CO₂ Electrolysis to Multicarbon Products at Activities Greater Than 1 A cm⁻². *Science* **2020**, *367* (6478), 661−666.

(9) Nesbitt, N. T.; Burdyny, T.; Simonson, H.; Salvatore, D.; Bohra, D.; Kas, R.; Smith, W. A. Liquid-Solid Boundaries Dominate Activity of CO₂ Reduction on Gas-Diffusion Electrodes. *ACS Catal.* **2020**, *10* (23), 14093−14106.

(10) Rabiee, H.; Ge, L.; Zhang, X.; Hu, S.; Li, M.; Yuan, Z. Gas Diffusion Electrodes (GDEs) for Electrochemical Reduction of Carbon Dioxide, Carbon Monoxide, And Dinitrogen to Value-Added Products: A Review. *Energy Environ. Sci.* **2021**, *14* (4), 1959−2008.

(11) Lees, E. W.; Mowbray, B. A. W.; Parlane, F. G. L.; Berlinguette, C. P. Gas Diffusion Electrodes and Membranes for CO₂ Reduction Electrolysers. *Nat. Rev. Mater.* **2022**, *7* (1), 55−64.

(12) Nguyen, T. N.; Dinh, C.-T. Gas Diffusion Electrode Design for Electrochemical Carbon Dioxide Reduction. *Chem. Soc. Rev.* **2020**, *49* (21), 7488−7504.

(13) Li, M.; Idros, M. N.; Wu, Y.; Burdyny, T.; Garg, S.; Zhao, X. S.; Wang, G.; Rufford, T. E. The Role of Electrode Wettability in Electrochemical Reduction of Carbon Dioxide. *J. Mater. Chem. A* **2021**, *9* (35), 19369−19409.

(14) Kim, C.; Bui, J. C.; Luo, X.; Cooper, J. K.; Kusoglu, A.; Weber, A. Z.; Bell, A. T. Tailored Catalyst Microenvironments for CO₂ Electroreduction to Multicarbon Products on Copper Using Bilayer Ionomer Coatings. *Nat. Energy* **2021**, *6* (11), 1026−1034.

(15) Kusoglu, A.; Weber, A. Z. New Insights into Perfluorinated Sulfonic-Acid Ionomers. *Chem. Rev.* **2017**, *117* (3), 987−1104.

(16) Mauritz, K. A.; Moore, R. B. State of Understanding of Nafion. *Chem. Rev.* **2004**, *104* (10), 4535−4586.

(17) Nwabara, U. O.; Hernandez, A. D.; Henckel, D. A.; Chen, X.; Cofell, E. R.; de-Heer, M. P.; Verma, S.; Gewirth, A. A.; Kenis, P. J. A. Binder-Focused Approaches to Improve the Stability of Cathodes for CO₂ Electroreduction. *ACS Appl. Energy Mater.* **2021**, *4* (5), 5175−5186.

(18) Junge Puring, K.; Siegmund, D.; Timm, J.; Möllenbruck, F.; Schemme, S.; Marschall, R.; Apfel, U.-P. Electrochemical CO₂ Reduction: Tailoring Catalyst Layers in Gas Diffusion Electrodes. *Adv. Sustainable Syst.* **2021**, *5* (1), 2000088.

(19) Pham, T. H. M.; Zhang, J.; Li, M.; Shen, T.-H.; Ko, Y.; Tileli, V.; Luo, W.; Züttel, A. Enhanced Electrocatalytic CO₂ Reduction to C₂₊ Products by Adjusting the Local Reaction Environment with Polymer Binders. *Adv. Energy Mater.* **2022**, *12* (9), 2103663.

(20) Bui, J. C.; Kim, C.; King, A. J.; Romiluyi, O.; Kusoglu, A.; Weber, A. Z.; Bell, A. T. Engineering Catalyst-Electrolyte Microenvironments to Optimize the Activity and Selectivity for the Electrochemical Reduction of CO₂ on Cu and Ag. *Acc. Chem. Res.* **2022**, *55* (4), 484−494.

(21) Mowbray, B. A. W.; Dvorak, D. J.; Taherimakhsousi, N.; Berlinguette, C. P. How Catalyst Dispersion Solvents Affect CO₂ Electrolyzer Gas Diffusion Electrodes. *Energy Fuels* **2021**, *35* (23), 19178−19184.

(22) So, M.; Ohnishi, T.; Park, K.; Ono, M.; Tsuge, Y.; Inoue, G. The Effect of Solvent and Ionomer on Agglomeration in Fuel Cell Catalyst Inks: Simulation by the Discrete Element Method. *Int. J. Hydrogen Energy* **2019**, *44* (54), 28984−28995.

(23) Ngo, T. T.; Yu, T. L.; Lin, H.-L. Nafion-Based Membrane Electrode Assemblies Prepared from Catalyst Inks Containing Alcohol/Water Solvent Mixtures. *J. Power Sources* **2013**, *238*, 1−10.

(24) Ngo, T. T.; Yu, T. L.; Lin, H.-L. Influence of the Composition of Isopropyl Alcohol/Water Mixture Solvents in Catalyst Ink Solutions on Proton Exchange Membrane Fuel Cell Performance. *J. Power Sources* **2013**, *225*, 293−303.

(25) Lee, S.-J.; Yu, T. L.; Lin, H.-L.; Liu, W.-H.; Lai, C.-L. Solution Properties of Nafion in Methanol/Water Mixture Solvent. *Polymer* **2004**, *45* (8), 2853−2862.

(26) Guo, Y.; Pan, F.; Chen, W.; Ding, Z.; Yang, D.; Li, B.; Ming, P.; Zhang, C. The Controllable Design of Catalyst Inks to Enhance PEMFC Performance: A Review. *Electrochem. Energy Rev.* **2021**, *4* (1), 67−100.

(27) Kuhl, K. P.; Cave, E. R.; Abram, D. N.; Jaramillo, T. F. New Insights into the Electrochemical Reduction of Carbon Dioxide on Metallic Copper Surfaces. *Energy Environ. Sci.* **2012**, *5* (5), 7050−7059.

(28) Yeo, R. S. Dual Cohesive Energy Densities of Perfluorosulphonic Acid (Nafion) Membrane. *Polymer* **1980**, *21* (4), 432−435.

(29) Ma, C.-H.; Yu, T. L.; Lin, H.-L.; Huang, Y.-T.; Chen, Y.-L.; Jeng, U. S.; Lai, Y.-H.; Sun, Y.-S. Morphology and properties of Nafion membranes prepared by solution casting. *Polymer* **2009**, *50* (7), 1764−1777.

(30) Hoffmann, E.; Fischer, D.; Thoma, M.; Damm, C.; Lobaz, V.; Zhigunov, A.; Peukert, W. Impact of DAA/Water Composition on PFSA Ionomer Conformation. *J. Colloid Interface Sci.* **2021**, *582*, 883−893.

(31) Hayes, W. M. *CRC Handbook of Chemistry and Physics*, 97th ed.; CRC Press: 2016.

(32) Li, T.; Shen, J.; Chen, G.; Guo, S.; Xie, G. Performance Comparison of Proton Exchange Membrane Fuel Cells with Nafion and Aquivion Perfluorosulfonic Acids with Different Equivalent Weights as the Electrode Binders. *ACS Omega* **2020**, *5* (28), 17628−17636.

(33) Ozden, A.; Wang, Y.; Li, F.; Luo, M.; Sisler, J.; Thevenon, A.; Rosas-Hernández, A.; Burdyny, T.; Lum, Y.; Yadegari, H.; Agapie, T.; Peters, J. C.; Sargent, E. H.; Sinton, D. Cascade CO₂ Electroreduction Enables Efficient Carbonate-Free Production of Ethylene. *Joule* **2021**, *5* (3), 706−719.

(34) Johnston, C. M.; Lee, K.-S.; Rockward, T.; Labouriau, A.; Mack, N.; Kim, Y. S. Impact of Solvent on Ionomer Structure and Fuel Cell Durability. *ECS Trans.* **2009**, *25* (1), 1617−1622.

(35) Moukheiber, E.; De Moor, G.; Flandin, L.; Bas, C. Investigation of Ionomer Structure Through its Dependence on Ion Exchange Capacity (IEC). *J. Membr. Sci.* **2012**, *389*, 294−304.

(36) Welch, C.; Labouriau, A.; Hjelm, R.; Orler, B.; Johnston, C.; Kim, Y. S. Nafion in Dilute Solvent Systems: Dispersion or Solution? *ACS Macro Lett.* **2012**, *1* (12), 1403−1407.

(37) Mahoney, S. A.; Rufford, T. E.; Johnson, D.; Dmyterko, A. S. K.; Rodrigues, S.; Esterle, J.; Rudolph, V.; Steel, K. M. The Effect of Rank, Lithotype and Roughness on Contact Angle Measurements in Coal Cleats. *Int. J. Coal Geol.* **2017**, *179*, 302−315.

(38) Idros, M. N.; Li, M. *ContactAngle: Contact Angle Measurement.* 1st Version; Github, 2021.

(39) Wu, Y.; Garg, S.; Li, M.; Idros, M. N.; Li, Z.; Lin, R.; Chen, J.; Wang, G.; Rufford, T. E. Effects of Microporous Layer on Electrolyte Flooding in Gas Diffusion Electrodes and Selectivity of CO₂ Electrolysis to CO. *J. Power Sources* **2022**, *522*, 230998.

(40) Kim, T.-H.; Yi, J.-Y.; Jung, C.-Y.; Jeong, E.; Yi, S.-C. Solvent Effect on the Nafion Agglomerate Morphology in the Catalyst Layer of the Proton Exchange Membrane Fuel Cells. *Int. J. Hydrogen Energy* **2017**, *42* (1), 478−485.

(41) Lin, H.-L.; Yu, T. L.; Huang, C.-H.; Lin, T.-L. Morphology Study of Nafion Membranes Prepared by Solutions Casting. *J. Polym. Sci., Part B: Polym. Phys.* **2005**, *43* (21), 3044−3057.

(42) Yan, X.; Xu, Z.; Yuan, S.; Han, A.; Shen, Y.; Cheng, X.; Liang, Y.; Shen, S.; Zhang, J. Structural and Transport Properties of Ultrathin Perfluorosulfonic Acid Ionomer Film in Proton Exchange Membrane Fuel Cell Catalyst Layer: A Review. *J. Power Sources* **2022**, *536*, 231523.

(43) Gogoi, P.; Chattopadhyay, A.; Gooh Pattader, P. S. Toward Controlling Evaporative Deposition: Effects of Substrate, Solvent, and Solute. *J. Phys. Chem. B* **2020**, *124* (50), 11530−11539.

(44) Li, Y.-F.; Sheng, Y.-J.; Tsao, H.-K. Evaporation Stains: Suppressing the Coffee-Ring Effect by Contact Angle Hysteresis. *Langmuir* **2013**, *29* (25), 7802−7811.

(45) Paul, D. K.; Karan, K.; Docoslis, A.; Giorgi, J. B.; Pearce, J. Characteristics of Self-Assembled Ultrathin Nafion Films. *Macromolecules* **2013**, *46* (9), 3461−3475.

(46) Kushner, D. I.; Kusoglu, A.; Podraza, N. J.; Hickner, M. A. Substrate-Dependent Molecular and Nanostructural Orientation of Nafion Thin Films. *Adv. Funct. Mater.* **2019**, *29* (37), 1902699.

(47) de Sousa, L.; Harmoko, C.; Benes, N.; Mul, G. Optimizing the Ink Formulation for Preparation of Cu-Based Gas Diffusion Electrodes Yielding Ethylene in Electroreduction of CO₂. *ACS ES&T Engg* **2021**, *1* (12), 1649−1658.

(48) Berlinger, S. A.; McCloskey, B. D.; Weber, A. Z. Inherent Acidity of Perfluorosulfonic Acid Ionomer Dispersions and Implications for Ink Aggregation. *J. Phys. Chem. B* **2018**, *122* (31), 7790−7796.

(49) Modestino, M. A.; Kusoglu, A.; Hexemer, A.; Weber, A. Z.; Segalman, R. A. Controlling Nafion Structure and Properties via Wetting Interactions. *Macromolecules* **2012**, *45* (11), 4681−4688.

(50) Goswami, S.; Klaus, S.; Benziger, J. Wetting and Absorption of Water Drops on Nafion Films. *Langmuir* **2008**, *24* (16), 8627−8633.

(51) Dura, J. A.; Murthi, V. S.; Hartman, M.; Satija, S. K.; Majkrzak, C. F. Multilamellar Interface Structures in Nafion. *Macromolecules* **2009**, *42* (13), 4769−4774.

(52) Quéré, D. Wetting and Roughness. *Annu. Rev. Mater. Res.* **2008**, *38* (1), 71−99.

(53) Ramya, K.; Velayutham, G.; Subramaniam, C. K.; Rajalakshmi, N.; Dhathathreyan, K. S. Effect of solvents on the characteristics of Nafion/PTFE composite membranes for fuel cell applications. *J. Power Sources* **2006**, *160* (1), 10−17.

(54) Yang, K.; Kas, R.; Smith, W. A.; Burdyny, T. Role of the Carbon-Based Gas Diffusion Layer on Flooding in a Gas Diffusion Electrode Cell for Electrochemical CO2 Reduction. *ACS Energy Lett.* **2021**, *6* (1), 33−40.

(55) Wu, Y.; Charlesworth, L.; Maglaya, I.; Idros, M. N.; Li, M.; Burdyny, T.; Wang, G.; Rufford, T. E. Mitigating Electrolyte Flooding for Electrochemical CO2 Reduction via Infiltration of Hydrophobic Particles in a Gas Diffusion Layer. *ACS Energy Lett.* **2022**, *7* (9), 2884−2892.

(56) Wang, L.; Nitopi, S. A.; Bertheussen, E.; Orazov, M.; Morales-Guio, C. G.; Liu, X.; Higgins, D. C.; Chan, K.; Nørskov, J. K.; Hahn, C.; Jaramillo, T. F. Electrochemical Carbon Monoxide Reduction on Polycrystalline Copper: Effects of Potential, Pressure, and pH on Selectivity toward Multicarbon and Oxygenated Products. *ACS Catal.* **2018**, *8* (8), 7445−7454.

(57) Handoko, A. D.; Ong, C. W.; Huang, Y.; Lee, Z. G.; Lin, L.; Panetti, G. B.; Yeo, B. S. Mechanistic Insights into the Selective Electroreduction of Carbon Dioxide to Ethylene on Cu₂O-Derived Copper Catalysts. *J. Phys. Chem. C* **2016**, *120* (36), 20058−20067.

(58) Huang, J. E.; Li, F.; Ozden, A.; Sedighian Rasouli, A.; García de Arquer, F. P.; Liu, S.; Zhang, S.; Luo, M.; Wang, X.; Lum, Y.; Xu, Y.; Bertens, K.; Miao, R. K.; Dinh, C.-T.; Sinton, D.; Sargent, E. H. CO_2 Electrolysis to Multicarbon Products in Strong Acid. *Science* **2021**, *372* (6546), 1074−1078.

(59) Tan, Y. C.; Lee, K. B.; Song, H.; Oh, J. Modulating Local CO_2 Concentration as a General Strategy for Enhancing C-C Coupling in CO_2 Electroreduction. *Joule* **2020**, *4* (5), 1104−1120.